Design of Induction Gradiometer for MCG Measurement

Kunihisa Tashiro, Shin-ichiro Inoue, and Hiroyuki Wakiwaka

Department of Electrical and Electronic Engineering,
Shinshu University, Wakasato 4-17-1, Nagano, Japan
tashiro@shinshu-u.ac.jp

Abstract. This paper presents a design of an induction gradiometer for MCG measurement in our laboratory environment. The pickup coil consists of two air-core coil having a diameter of 12 cm, connected in a differential structure. With two simple equivalent circuit models, we emphasize the benefit of current detection model compared with voltage detection model. To address the problems in conventional current-to-voltage converter, we propose a differential structured current-to-voltage converter and a suitable grounding technique. For MCG measurement in our laboratory environment, we design a signal conditioning circuits for the electronics. The sensitivity is as high as 32.3 mV/pT when the frequency is higher than the cutoff frequency of 18 Hz. It is a challenge to detect MCG signal without magnetically shielded environment. To suppress environmental noise contained in the output voltage, we use digital filters and an averaging technique. Although the sensitivity is enough to detect MCG signal, the phase profile of the electronics distorts the original signal. With a modeled MCG signal generated by one-turn coil, the expected output signal is confirmed. Finally, we demonstrate the detection of magnetic field from a human heart in our laboratory environment.

1 Introduction

Recently, a lot of magnetic sensors are being presented by researchers [1]. Sensors which can detect a weak magnetic field are important for a variety of applications, such as magnetometers for space research, gradiometers for biomagnetism, current sensors for hybrid vehicles, etc. The objective of this study is the development of a portable magnetic sensor which can detect weak magnetic fields in the low frequency range. In order to detect magnetic fields of less than 1 pT, three kinds of detection methods are well known. The first detection method is the use of a superconducting quantum interference device (SQUID). Although a SQUID magnetometer is a standard tool for biomagnetic measurements, liquid nitrogen or helium and its maintenance are essential. The second detection method is the use of the Zeeman effect. While an optically pumped magnetometer is based on this method, the necessity of an alkali-metal vapor, a radio-frequency generator and a high power laser makes the system complicated. The third detection method is the use of Faraday's law, where an induction magnetometer detects the induced voltage of a pickup coil. Though most previous works mention magnetometers

S.C. Mukhopadhyay et al. (Eds.): Advancement in Sensing Technology, SSMI 1, pp. 139–164.
springerlink.com

through Faraday's law, an approach from the definition of self-inductance is important when the target of the magnetic field is weak and low-frequency. One reason for this is the necessity of an ideal analogue integrator which does not have 1/f noise, dc drift, and a limitation in gain [2].

We have been developing induction magnetometers based on the definition of inductance [3-8]. Our proposed design of the pickup coil is based on a Brooks coil [9]. This shape of the coil can achieve a maximum inductance for a given length of winding wire, and the estimation error of the inductance is less than 3 % [6]. Induction magnetometers have the ability to detect weak magnetic fields from extremely low frequencies to those in the audible range (0.01 Hz ~ 10 kHz). Although induction magnetometers were proposed in several papers [1-2, 10-15], the technical details were usually not described. Because the nature of the coil is a fundamental basis of electromagnetism, the principles of induction magnetometers are easy to understand. However, the optimization of their design with numerous parameters is not easy. In order to simplify the design for the general shape of a pickup coil, we pay attention to the important relationships between flux linkage, current and voltage. In our previous report [7], we had determined four operation modes of a magnetometer which can be categorised with two detection models and two frequency ranges. The equivalent circuits for operation modes are based on Faraday's law, the definition of inductance, and Ohm's law. Some experimental results also showed the validity of these models. Previous systems [3-7] used a conventional current-to-voltage converter in the electronics. We have already reported that our sensor is very sensitive to electrical interference, and a suitable grounding point for the electronics is definitely required for detecting a weak magnetic field [16]. Therefore, we could not use the real performance of the magnetometer.

The purpose of this study is to demonstrate magnetocardiography (MCG) measurements obtained from a human heart. Magnetic field signals from the human heart were first detected by Baule and MacFee in 1963 [17]. Cohen detected magnetic fields outside of the human scalp in a multilayer magnetically shielded room [18]. In recent years, biomagnetism measurements have received considerable attention for the early detection of heart diseases. SQUID sensors are mostly used in real-time MCG measurements. This sensor is highly-sensitive but requires liquid helium/nitrogen during measurements [19]. Although the magnetically shielded room can provide a suitable environment for MCG measurement [20], it is extremely expensive, heavy, and practical problems. It is a challenge to detect MCG signal with simple instrumentations. In order to detect MCG signal in our laboratory environment, we designed an induction gradiometer. The pickup coil consists of two Brooks coils having a diameter of 120 mm which is connected in a differential structure [16]. Because this structure of the coil cannot detect a uniform magnetic field, it can help to suppress magnetic environmental noise contained in the output voltage.

First of all, we explained the operation principle of the induction gradiometer with two simple equivalent circuit models. Assuming the mutual inductance of two Brooks coils to be zero, the models are similar as the induction magnetometer [7]. According to the simulated results with LTSpice, we proposed a differential structured current-to-voltage converter. Compared with the conventional converter, the influence of grounding perturbation on the output voltage was found to be

insignificant. By using a Faraday cage to provide an electrically shielded space, we investigated electrical interference to the gradiometer. As a result, it was found that the electrical interference to the new converter with a dummy load was negligible. We identified that the dominant electrical interference was caused by electrical field of 60 Hz, the power-line frequency, to the pickup coil. With a suitable grounding condition, there was no significant electrical interference. The noise floor level of the gradiometer and the typical magnetic field of 60 Hz which appeared in the output voltage were also confirmed. Based on the preliminary results, we redesigned the electronics in the gradiometer for MCG measurement. Simulated results by LTSpice were in good agreement with the design. Although the sensitivity was enough to detect MCG signal, it was expected that the phase profile of the electronics may distort the original signal. With a modeled MCG signal generated by one-turn coil, we confirmed the possibility to detect MCG signal. By employing method such as digital filters and averaging technique, we successfully observe the corresponding signal of 0.9 $V_{p\text{-}p}$ when the value of R-wave in the modeled signal was 100 $pT_{p\text{-}p}$. Finally, we demonstrated the detection of magnetic field near the chest of a human subject in our laboratory environment.

2 Equivalent Circuit Model

Fig. 1(a) shows a model based on Faraday's law. We assume that a homogeneous magnetic flux B [T] of frequency f [Hz] is crossed with a coil having mean radius a [m]. The induced voltage V [V] is expressed by the following equation.

$$V = -(\mathrm{d}\Phi / \mathrm{d}t) = -\mathrm{j}2\pi^2 f n a^2 B \quad [\mathrm{V}] \tag{1}$$

Where j is an imaginary number and n is the number of coil windings. When we measure the voltage and integrate it with an ideal integrator, we can obtain the waveform of the magntic flux density. Fig. 1(b) shows a model based on the definition of inductance. The relationship between the current I [A] and flux linkage Φ is expressed by the following equation.

$$\Phi = L I \quad [\mathrm{Wb}] \tag{2}$$

$$I = (nSB)/L = (\pi n a^2 B) / L \ [\mathrm{Wb}] \tag{3}$$

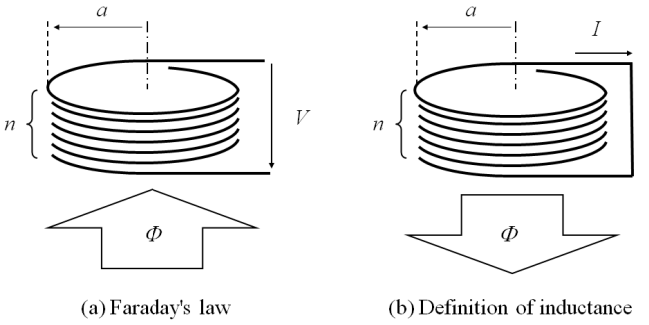

Fig. 1. Faraday's law and definition of inductance

Where L [H] is the inductance of the coil. When we measure the induced current, we can obtain the waveform of the magntic flux density. However, it should be disscussed with a finite resistance in the coil and instrumentation. Here, we consider that a pickup coil consists of two coils. The self-inductance and resistance of the coil are L_s and R_s, respectively. The coils are connected in differential structure. If the distance between two coils is relatively large, the mutual inductance is neglected. The total inductance and resistance of the pickup coil are $L = 2L_s$ and $R = 2R_s$, respectively. When a homogeneous magnetic flux is crossed with both coil, the same induced voltages appear in both coil. Because the coils are connected in differential structure, the voltages are cancelled. Therefore, a current is not induced in the pickup coil if the terminal of pickup coil is shorted. However, an induced current appears in the pickup coil if there is an imbalance of magnetic flux density in the pickup coil. We can also express the induced voltage of the pickup coil by eq(1).

Fig. 2 shows the voltage detection model. A homogeneous magnetic flux is crossed with one coil. The induced voltage is measured using instrumentation which has an input resistance of R_{in} [Ω]. Based on Thevenin's theorem, the pickup coil can be replaced with parameters of R, L, and V [7].

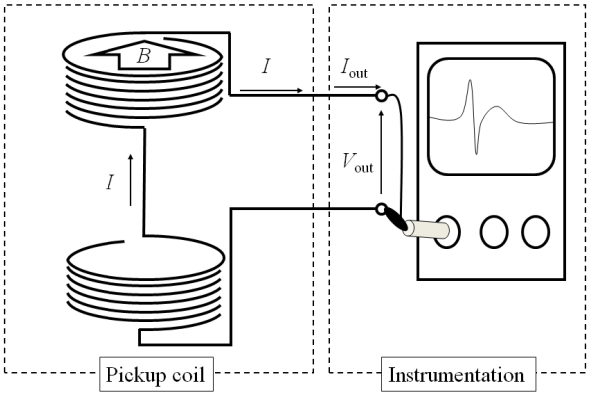

(a) Model

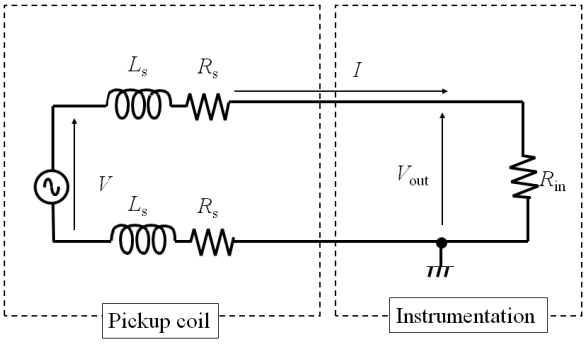

(b) Equivalent circuit

Fig. 2. Induced voltage detection model

Fig. 3 shows the current detection model with a current-to-voltage converter having a transimpedance gain, or a feedback resistance, R_f [Ω]. Because the plus pin of the opamp is connected to the ground, the input resistance is zero and the pickup coil is in a virtual short. The output voltage of the current-to-voltage converter is the product of R_f and I.

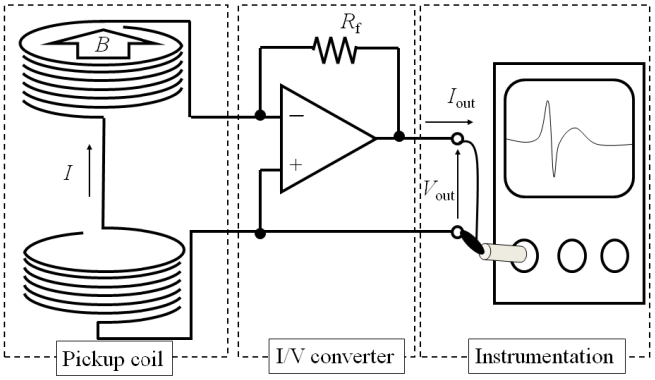

(a) Model

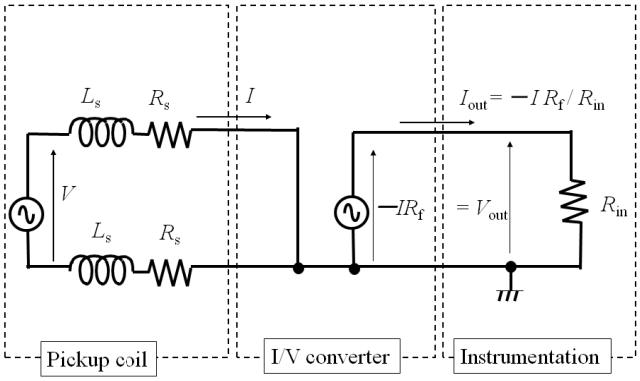

(b) Equivalent circuit

Fig. 3. Induced current detection model

The frequency response of the magnetometers can be considered by two frequency regions where the resistance or the inductance is dominant. Because the equivalent circuits of both detection types are regarded as a simple RL circuit, cutoff frequencies f_v and f_i can be defined.

$$f_v = R_{in} / (2\pi L) \quad \text{[Hz]} \quad \text{(For voltage detection model)} \tag{4}$$

$$f_i = R / (2\pi L) \quad \text{[Hz]} \quad \text{(For current detection model)} \tag{5}$$

When the frequency range is smaller than its own cutoff frequency, the output voltage is proportional to the frequency.

$$V_{out} = -j2\pi^2 f n a^2 B \quad [V] \qquad \text{(For voltage detection model)} \tag{6}$$
$$V_{out} = -(R_f/R) \times j2\pi^2 f n a^2 B \quad [V] \qquad \text{(For current detection model)} \tag{7}$$

When the frequency range is higher than its own cutoff frequency, the output voltage does not depend on the frequency.

$$V_{out} = -\pi n a^2 R_{in} B / L \quad [V] \text{ (For voltage detection model)} \tag{8}$$
$$V_{out} = -\pi n a^2 R_f B / L \quad [V] \text{ (For current detection model)} \tag{9}$$

Here, we define $|V / B|$ [V/T] as the sensitivity of the magnetometer. The sensitivity of both detection models is limited in the high frequency region. If we assumed that $R_f = R_{in}$, the sensitivities in the high frequency regions are the same. In order to simplify the equations of the sensitivity, we introduced two symbols.

$$F = 2\pi^2 f n a^2 \text{ [V/T]} \tag{10}$$
$$G = (R_f \pi n a^2) / L = (R_{in} \pi n a^2) / L \text{ [V/T]} \tag{11}$$

In this paper, we used a pickup coil which consists of two Brooks coils. This shape of the coil can achieve maximum inductance for a given length of winding wire, and the estimation error of the inductance is very low[9]. It is also known that the estimation method of mutual inductance between two Brooks coils. If the distance between the two coil is 10 times larger than the coil width, the mutual inductance is negligible. The value is 0.3 % compared with the self-inductance of one coil. Table 1 shows the specifications of our developed pickup coil for consideration in this paper.

Table 1. Specifications of the induction gradiometer

Property	Value
Brooks coil	
Mean diameter, a[m]	0.045
Coil width, c [m]	0.030
Inner diameter, $2c$ [m]	0.060
Outer diameter, $4c$ [m]	0.120
Number of windings, n [turn]	2827
Diameter of the wire, δ [m]	0.5×10^{-3}
Estimated resistivity of the wire, ρ [Ω m]	1.78×10^{-8}
Coil constant, P_0 [H/m]	1.6994×10^{-6}
Self inductance, $L_s = P_0 an^2$[H]	0.61
Resistance, $R_s = 2\pi an\rho / ((\delta/2)^2\pi)$ [Ω]	72
Induced voltage, $V = -j2\pi^2 fna^2 B$[V]	$-j113fB$
Pickup coil	
Distance between Brooks coils, l [m]	0.3
Inductance, $L = 2Ls$ [H]	1.22
Resistance, $R = 2R_s$ [Ω]	144
Cutoff frequency, $f_i = R / 2\pi L$ [Hz]	18.5
Sensitivity $(R_f/R)\times F = (R_f/R) \times 2\pi^2 fna^2$ [V/T]	$0.796 R_f f$
Sensitivity $G = R_f \pi n a^2 / L$ [V/T]	$14.7R_f$

The outer diameter is 120 mm, the inner diameter is 60 mm, the coil width is 30 mm, and the number of windings is 2827 with a copper wire of 0.2 mm in diameter. The distance between the two coils is 300 mm. Fig. 4 illustrates an example of the frequency response of the sensitivity for the two detection models. Both models require different methodologies for optimal pickup coil design. In the low frequency region, the sensitivity of the current detection model is (R_f /R) times than that of the voltage detection model. Although an increase in n makes the sensitivity large in the voltage detection model, the value of R becomes large. Because Johnson noise is proportional to $R^{1/2}$, the noise floor level of the magnetometer becomes worse. Although we can use a voltage amplifier in the voltage detection model, it should be noted that we can use a quite high the ratio of the transimpedance gain to the pickup coil resistance, R_f /R, in the current detection model. According to the considerations of the equivalent circuit model, an estimation of the resistance and inductance is very important for the design.

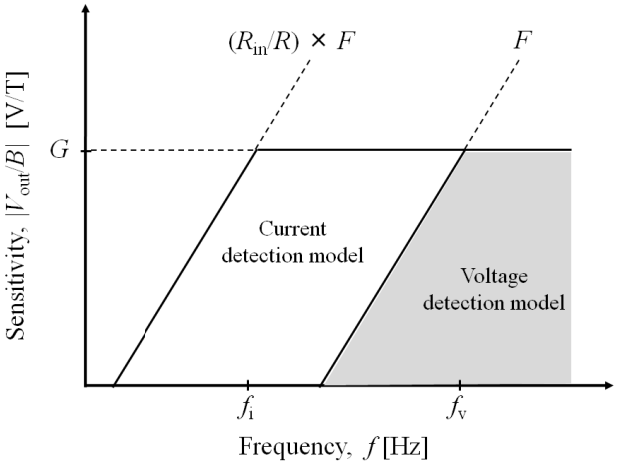

Fig. 4. Theoretical frequency response of the sensitivity for the two detection model

3 Current-to-Voltage Converter

Our proposed equivalent circuit model allows us to analyze the gradiometer with a circuit simulator, LTSpice(Linear technology Inc.). This simulator can reproduce the real properties of an op-amp made by Liner Technology faithfully. We have already reported two problems in current detection type induction magnetometers from previous experimental results. This kind of magnetometer is sensitive to power line noise and electrical interference, because the impedance of an equivalent circuit for the pickup coil is very low [16].

Fig. 5 shows the model with a conventional current-to-voltage converter for LTSpice. Because the feedback resistor R_f is 1 MΩ, the transimpedance gain is 1×10^6 V/A. In this model, practical conditions were also considered. In the power supply, a voltage source named “Perturbation” represents a disturbance in

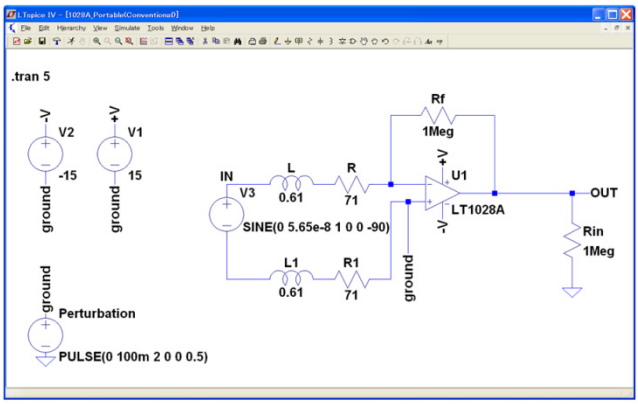

Fig. 5. A LTSpice model for a conventional current-to-voltage converter

grounding voltage. The voltage source in the pickup coil represents magnetic field crossing the pickup coil, which is expressed by eq. (1). A voltage source of 56.5 nV at 1 Hz corresponds to 1 $nT_{p\text{-}p}$.

Fig. 6 shows an example of a simulated output voltage waveform. The grounding voltage disturbance was not added. The output voltage for the magnetic field of 1 $nT_{p\text{-}p}$ at 1 Hz was 0.8 $mV_{p\text{-}p}$, which is same value as expected from eq (7). Fig. 7 shows the output voltage as a function of frequency for a magnetic field of 1 $nT_{p\text{-}p}$. The solid line represents the results simulated by LTSpice, and the dashed line represents our design with theoretical estimation. The simulated frequency response was similar as our expected. Fig. 8 shows an example of simulated output voltage waveform, which takes into account the unstable grounding.

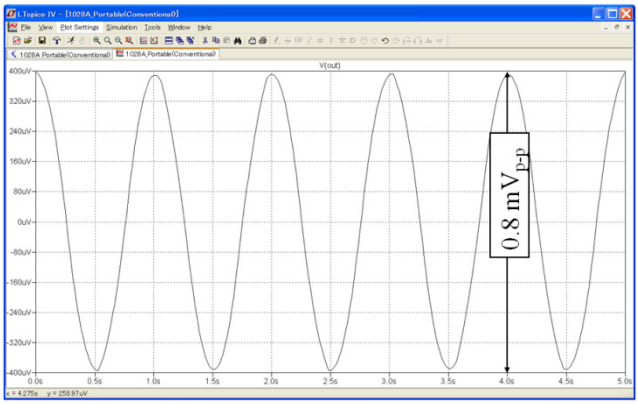

Fig. 6. Simulated output voltage waveform for a magnetic field of 1 $nT_{p\text{-}p}$ at 1 Hz. The grounding voltage disturbance was not added.

When a pulse voltage of 100 mV from 2 s to 2.5 s was added to the ground, the perturbation of the ground level appeared the output voltage, directly. Through an

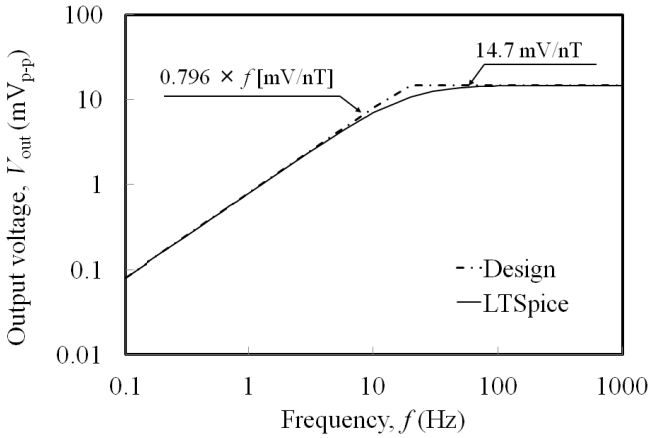

Fig. 7. Output voltage as a function of frequency for a magnetic field of 1 nT$_{p-p}$

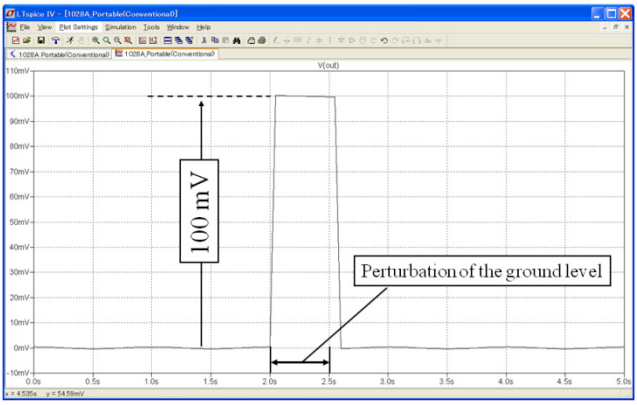

Fig. 8. Simulated output voltage waveform for a magnetic field of 1 nT$_{p-p}$ at 1 Hz. A pulse voltage of 100 mV from 2.0 s to 2.5 s was added to the ground.

experiment with a Faraday cage, we have already noticed the necessity for a suitable grounding point for electronics. However, some improvement of electronics should be considered to suppress the influence. If the sensor is based on a voltage detection model, an instrumentation amplifier is a suitable choice. It has good linearity gain even if it is under electrically noisy conditions. The most famous instrumentation amplifier consists of three op-amps. The input stage of the amplifier is a differential structure with two op-amps, which has the ability of common mode noise reduction. From these considerations, we propose a differential-input type current-to-voltage converter. To the best of the authors' knowledge, some structures of a differential input stage were proposed by other researchers [16-17]. However, we don't know this kind of a new structured circuit design for induction gradiometers.

Fig. 9 shows the model with a differential-input type current-to-voltage converter for LTSpice. The induced current in the pickup coil is converted into a

voltage with a differential-input type current-to-voltage converter. Because of the differential structure, the transimpedance gain is 2×10^6 V/A. Fig. 10 shows an example of a simulated output voltage waveform with the new converter. Although a pulse voltage of 100 mV from 2 s to 2.5 s was added to the ground, there was no significant disturbance in the waveform. The output voltage for a magnetic field of 1 n $pT_{p\text{-}p}$ at 1 Hz was 1.6 $mV_{p\text{-}p}$. It should be noted that the output voltage is twice compared with that of the conventional converter.

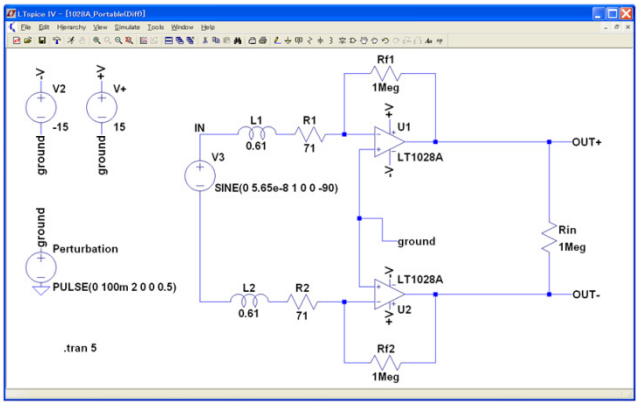

Fig. 9. A LTSpice model for differential-input type current-to-voltage converter

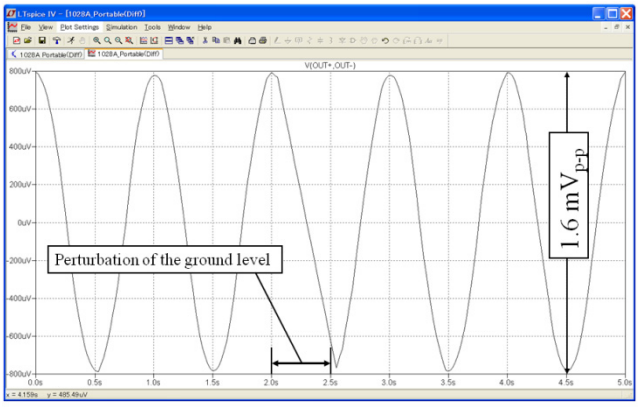

Fig. 10. Simulated output voltage waveform for a magnetic field of 1 $nT_{p\text{-}p}$ at 1 Hz. A pulse voltage of 100 mV from 2.0 s to 2.5 s was added to the ground.

4 Electrical Interference

According to the LTSpice simulation results, we confirmed that a grounding perturbation did not affect the output voltage of a differential-input type current-to-voltage converter. However, the source of the electrical interference is not unknown. In order to reveal the source, we conducted experiments with a Faraday cage.

Fig. 11 shows our constructed Faraday cage. It consists of copper mesh and wood, and is 2.0 m × 1.8 m × 1.8 m in size. The copper mesh size is 2 mm, and the diameter of the copper wire 0.45 mm. No magnetic materials are used for avoiding magnetic noise. We evaluated electric noise in our laboratory room environment using a battery powered oscilloscope (TPS2014, Textronics) and a typical voltage probe. Fig. 12 shows the evaluated laboratory rooms. (a) shows the typical laboratory room (Room 403), (b) shows a room (Room 408) where the Faraday cage is built. The measuring height is 1 m from the floor, and the measuring spacing is 0.2 m. The measured value of voltage is divided by probe distance (70 mm), and converted into units of electrical field.

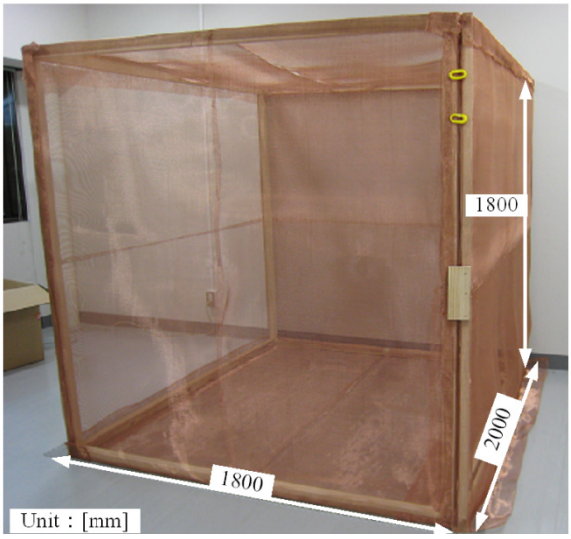

Fig. 11. Our constructed Faraday cage

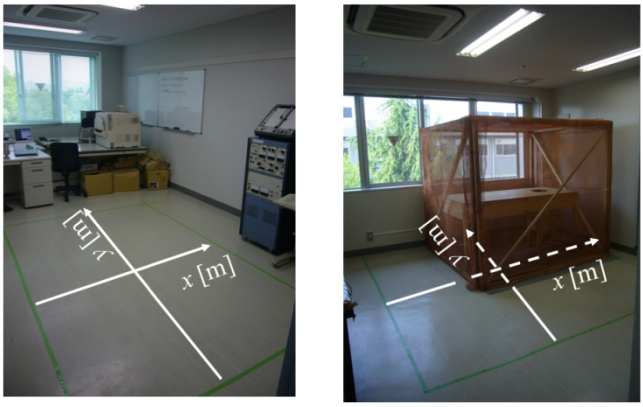

(a) Room 403 (b) Room 408

Fig. 12. Our laboratory's rooms

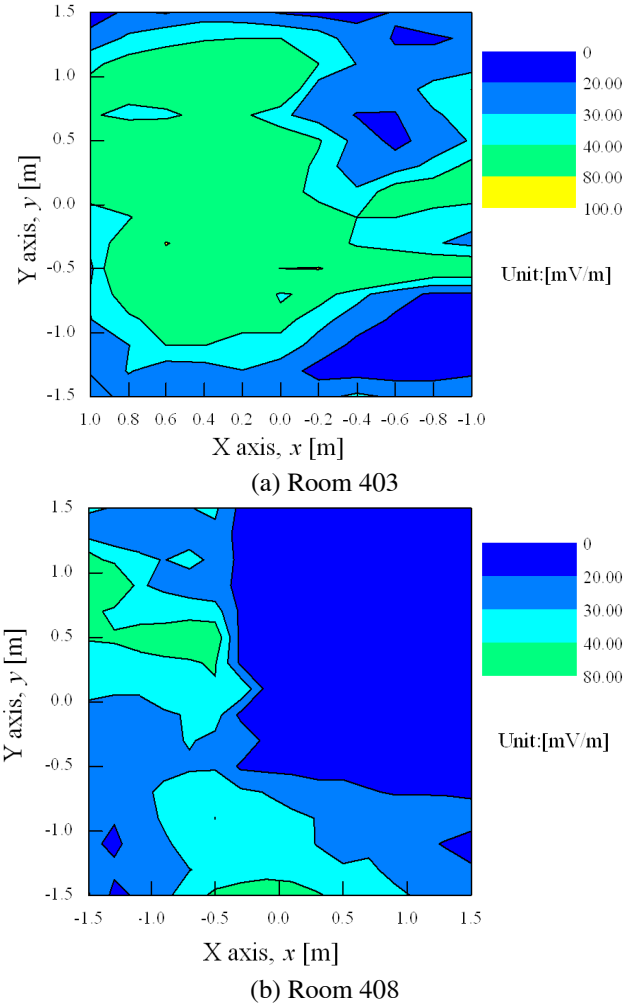

Fig. 13. Measured electrical field distributions

Fig. 13(a) shows the measured electrical field distribution in Room 403. The typical field was larger than 40 $mV_{p\text{-}p}/m$. After various traials, it was found that the primary source of noise was room light and the frequency component was 60 Hz. The measured field near the room light was larger than 200 $mV_{p\text{-}p}/m$. Fig. 13(b) shows the measured electrical field distribution in Room 403. We also confirmed that the field was large where the measuring point was under a light source. In contrast, the field inside the Faraday cage was less than 20 $mV_{p\text{-}p}/m$. In order to evaluate the magnetic shielding effect for low frequency fields of the cage, we measured magnetic noise using a fluxgate sensor (uMag-01, MEDA). The fluxgate sensor is placed on the wooden base. The measured value of geomagnetic field is

similar as 23 μT at both rooms. The measured amplitude of power line noise is also similar, as 10 to 100 nT, at the both Rooms. The differences in the amplitude were not larger than ten times between inside and outside of the cage. It means that the magnetic shielding effect of the cage was negligible.

Fig. 14 shows a schematic design of an induction gradiometer to investigate the electrical interference. The equivalent circuit is same as shown in Fig. 8 whose transimpedance gain is 2×10^6. We focused on the 60 Hz component of the output voltage, because it was the dominant frequency component of the electrical field. First of all, we used a dummy load instead of the pickup coil. The waveform of the output voltage was measured by the oscilloscope, and analyzed by FFT. The ideal output voltage is, needless to say, zero. However, an increase in the resistance produces an increase in thermal noise (Johnson noise) [6].

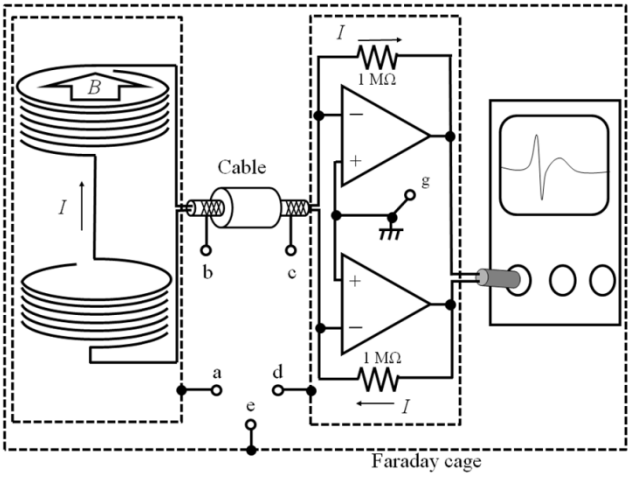

Fig. 14. Schematic design of an induction gradiometer to investigate the electrical interference

Fig. 15 shows an example of the FFT analysis result of the measured output voltage. The sensitivity of the sensor is 2.94×10^7 V/T where the frequency is higher than the cutoff frequency of 18 Hz. Because the noise floor level was about 0.1 mV, the corresponding noise floor level of the induction gradiometer was 3.4 pT. While this oscilloscope cannot analyze the output voltage of less than 0.1 mV, we confirmed that no electrical interference was observed which corresponded to the magnetic field of a few pT. It should be noted that there were no significant differences if the converter was placed outside of the Faraday cage.

Fig. 16 shows a photograph of the induction gradiometer. A battery is used for the DC power supply to the current-to-voltage converter. The point “a” and “d” represent the contacting points on the electrical shield for the pickup coil and the converter. The points “b” and “c” represent the contacting point on the cupper

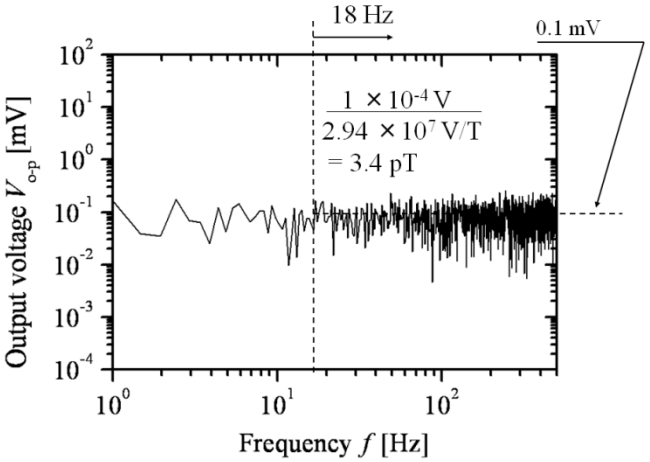

Fig. 15. An example of the FFT analysis result of the measured output voltage

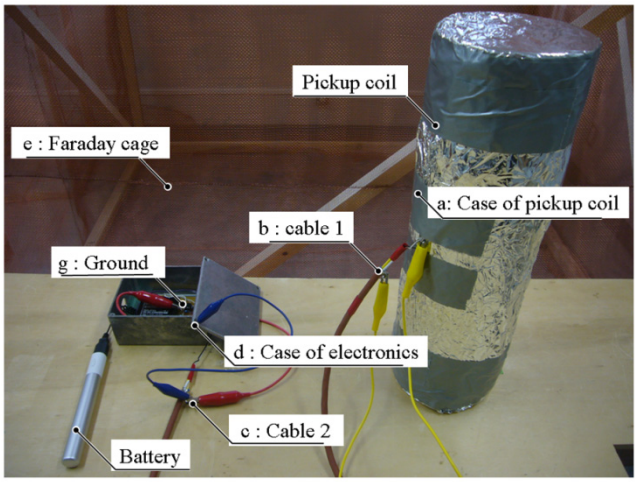

Fig. 16. Our developed induction gradiometer

mesh layer of the cable. The point "e" represents the contacting point on the Faraday cage. The point "g" represents the grounding point of the converter. The resistance values of the cables, used for the connecting points, are less than 0.2 Ω. In the previous presentation at ICST2011 [21], we investigated a suitable grounding point without the Faraday cage for practical use.

As a result, it was found that the output waveform was dramatically changed due to electrical interference to the pickup coil when the all connecting points were not connected. Fig. 17(a) shows an example of the observing output waveform outside the Faraday cage. All connecting points were not connected. The peak-to-peak voltage was about 400 mV, and the dominant frequency

component was power-line frequency of 60 Hz. In contrast, the peak-to-peak voltage was reduced about 1/20 when the gradiometer was placed inside the cage. It means that the difference in the output voltage was caused by electrical interference to the pickup coil. In contrast, there was no difference when all the connecting points were connected. Fig. 17(b) shows an example of the observing output waveform outside the cage. No significant difference was observed when the gradiometer was placed inside the cage. The peak-to-peak voltage was about 20 mV, and the corresponding magnetic flux density was 0.68 $nT_{p\text{-}p}$.

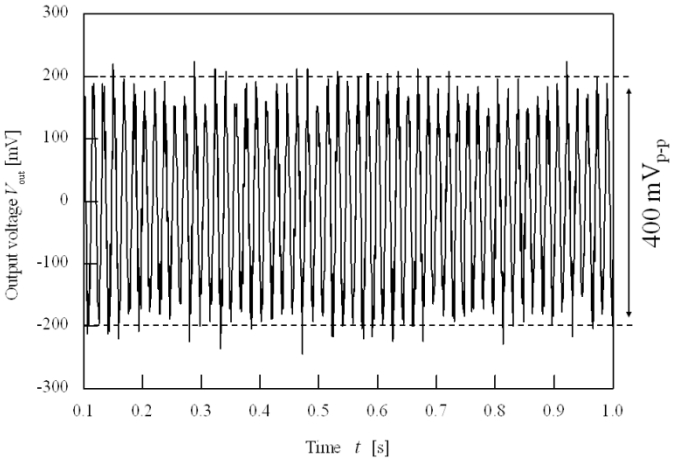

Fig. 17. (a) An example of the observing output waveform outside the Faraday cage. All connecting points were not connected.

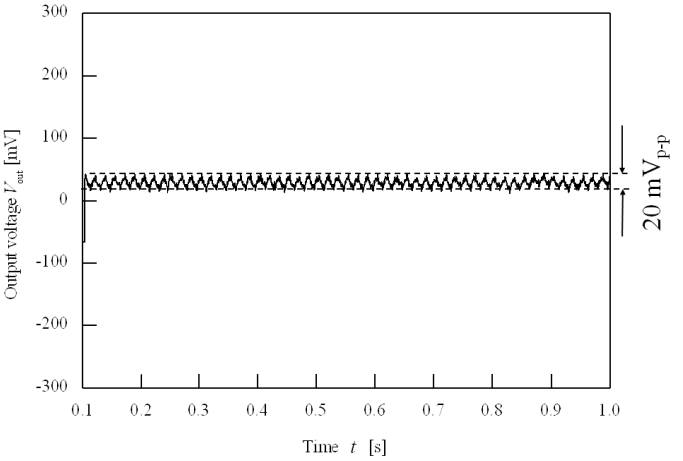

Fig. 17. (b) An example of the observing output waveform outside the Faraday cage. All connecting points were connected.

5 Electronics Design

For the observation of MCG signal from a human heart as low as 100 $pT_{p\text{-}p}$, we designed the electronics for the induction gradiometer. Fig. 18 shows a model of the electronics for LTSpice. The transimpedance gain of the current-to-voltage converter is 2×10^7 V/A which is ten times larger than before. A differential-input type HPF is also inserted to reject a finite offset voltage, and the cutoff frequency of both filters was set to 0.3 Hz. The gain of the final amplifier is 110.

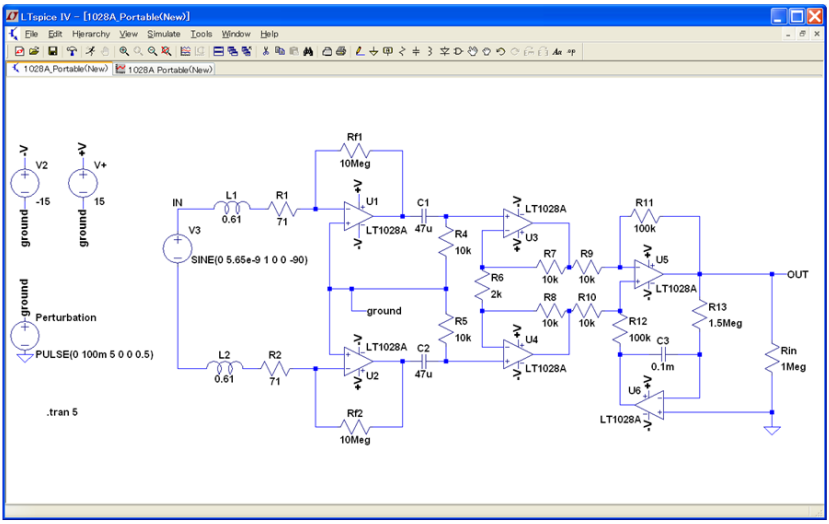

Fig. 18. A model of the electronics for the induction gradiomter

Fig. 19 shows an example of a simulated output voltage waveform with the new electronics. A voltage source of 5.65 nV at 1 Hz corresponds to 100 $pT_{p\text{-}p}$. For the demonstration of the grounding disturbance, a pulse voltage of 100 mV from 2 s to 2.5 s was added to the ground. There was no significant disturbance due to the grounding perturbation, and the output voltage for a magnetic field of 100 $pT_{p\text{-}p}$ at 1 Hz was 164 $mV_{p\text{-}p}$. We can see that a transient response due to the filters was observed rapidly. Fig. 20 shows the output voltage as a function of frequency for a magnetic field of 100 $pT_{p\text{-}p}$. Line represents the results simulated by LTSpice, and the dashed line represents our design with theoretical estimation. Although the simulated frequency response was as similar as our expected, the phase profile was changed due to the filters. Fig. 21 shows the phase profile as a function of frequency. The solid line represents the results with the new electronics, and the dashed line represents the current-to-voltage converter. It means that the detected signal would be distorted compared with the original MCG signal.

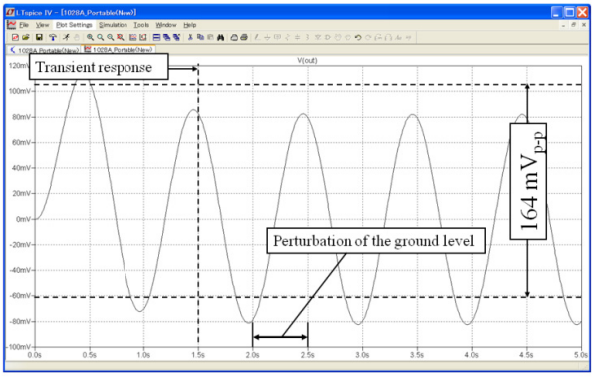

Fig. 19. Simulated output voltage waveform for a magnetic field of 100 pT_{p-p} at 1 Hz

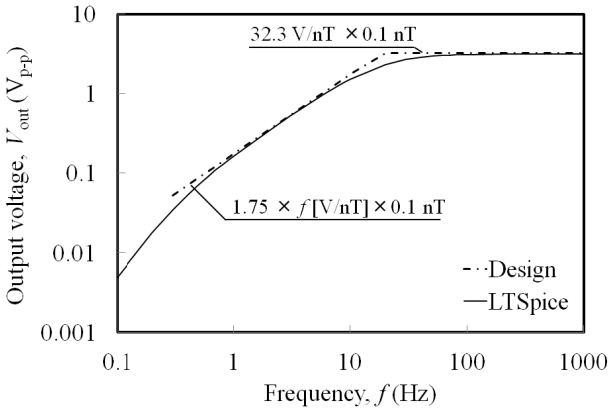

Fig. 20. Output voltage as a function of frequency for a magnetic field of 100 pT_{p-p}

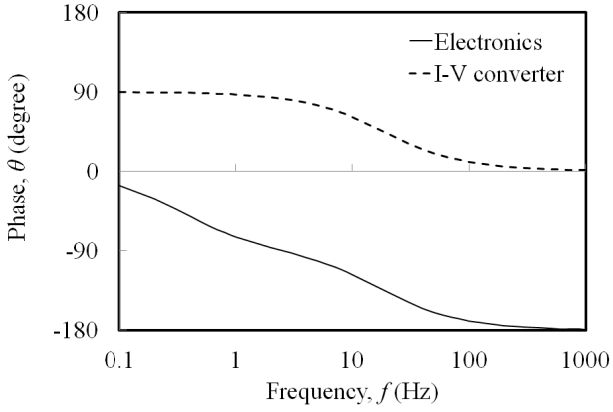

Fig. 21. Phase profile as a function of frequency

In order to check the expected output voltage waveform for the MCG signal, we demonstrated MCG measurement with a modelled MCG signal. One-turn coil of 14 cm diameter was used for generating a modelled MCG signal. A fluxgate sensor was set 2 cm away from the one-turn coil. We confirmed the relationship in the one-turn coil between generated magnetic field and applied current. From an experimental result, 120 mA_{p-p} generated magnetic field of 100 nT_{p-p}. We applied the modelled MCG signal to the one-turn coil using LabVIEW. In order to generate the signal whose R-wave peak amplitude became 1 nT_{p-p} and 100 pT_{p-p}, we set the current value of 1.2 mA and 0.12 mA. Fig. 22 and 23 show the experimental setup and schematic diagram of the measurement, respectively.

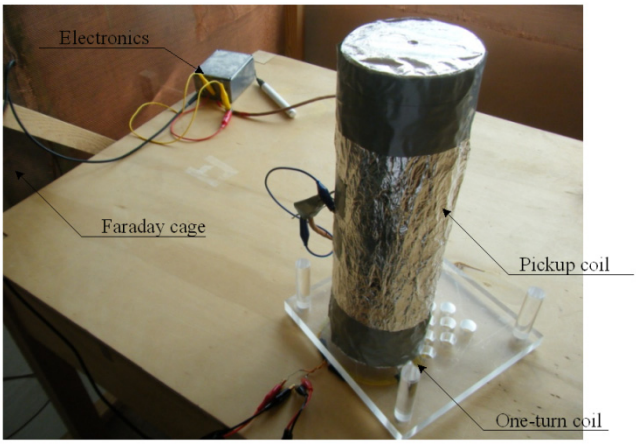

Fig. 22. Experimental setup for measurement of modelled MCG signal

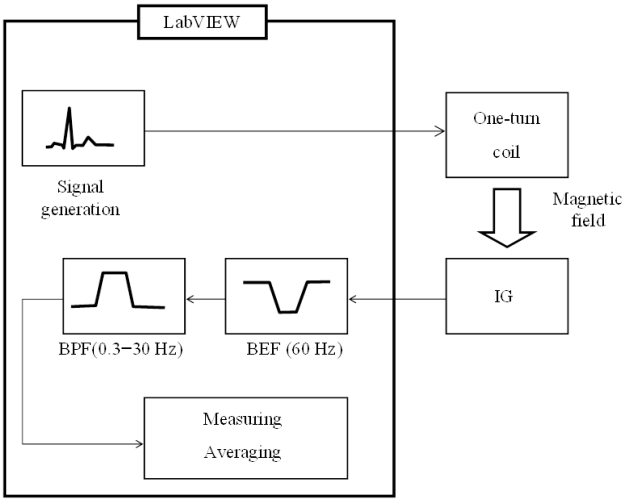

Fig. 23. Schematic design for measurement of modelled MCG signal

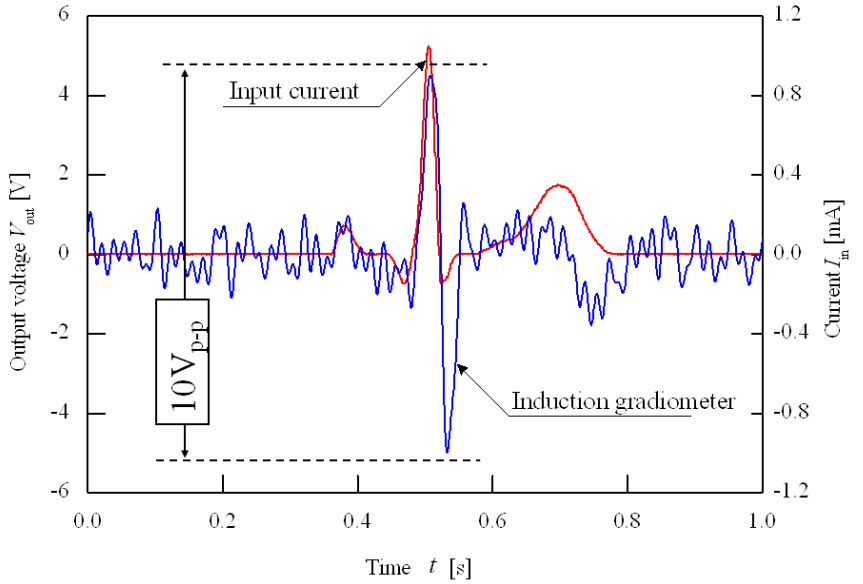

(a) R-wave of 1 nT_{p-p}

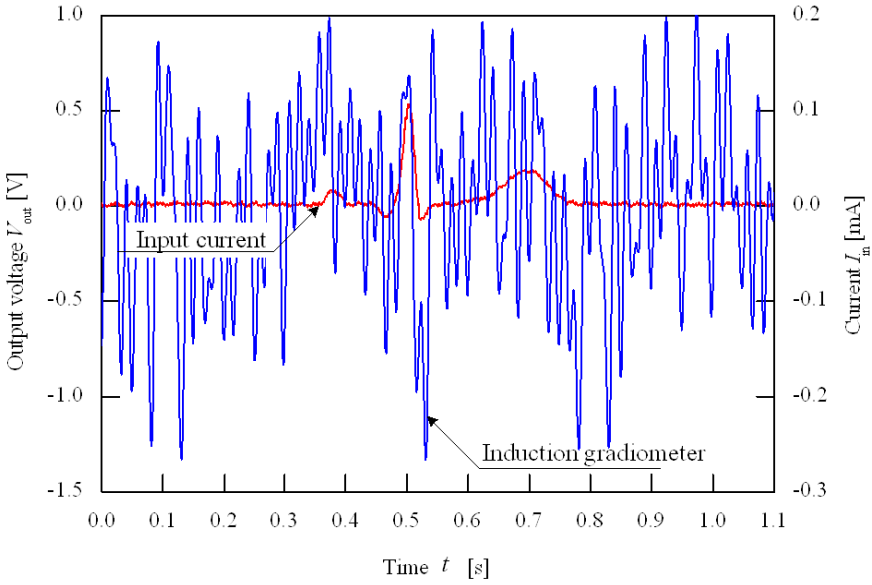

(b) R-wave of 100 pT_{p-p}

Fig. 24. Measured examples of the waveform for modelled MCG signal

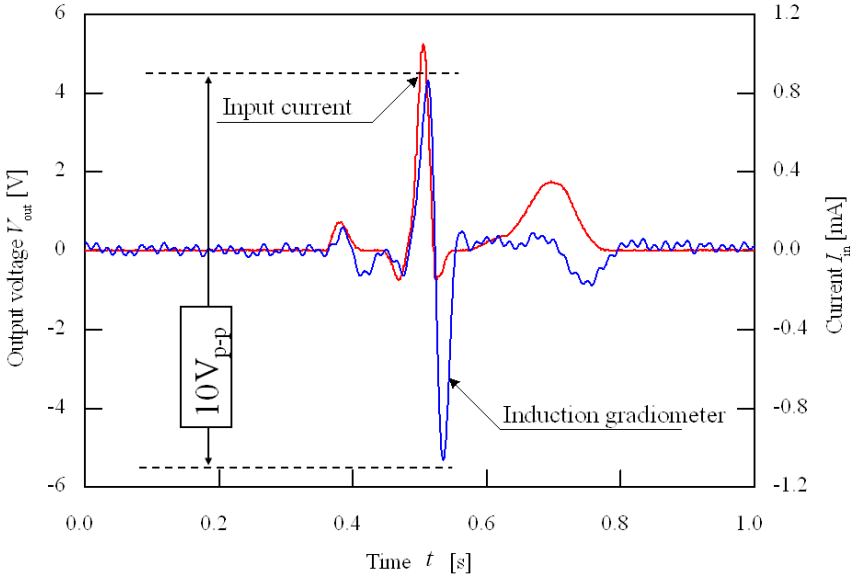

(a) R-wave of 1 nT_{p-p}

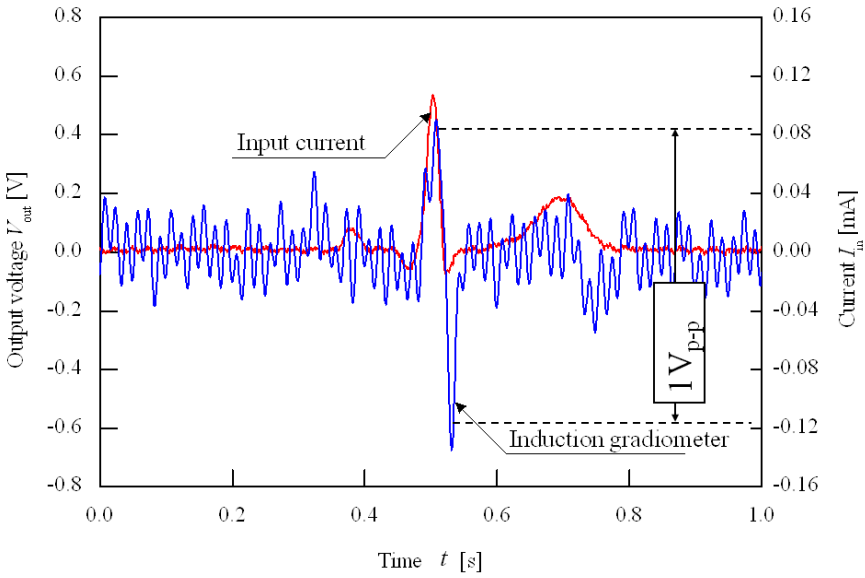

(b) R-wave of 100 pT_{p-p}

Fig. 25. Measured examples of the waveform for modelled MCG signal averaged 20 times

While the design of electronics for the induction magnetometer was as same as design mentioned before, we chose OP27 (Analog devices) for the op-amps in current-to-voltage converter. From our several considerations, the offset voltage in the output voltage with this op-amp was 10 times lower than that with LT1028A. The output signal of the gradiometer was processed by digital filter after the voltage was recorded by LabVIEW. Digital filters are band-pass filter (BPF) and band-eliminate filter (BEF). The cutoff frequency of this BEF corresponds to the power-line frequency of 60 Hz. This BPF allows passage of 0.3 ~ 30 Hz which corresponds to the frequency range of MCG signal.

Fig. 24 shows measured examples of the waveform for the modelled MCG signal. Although the output signal was distorted, we successfully observed the corresponding signal of 10 V_{p-p} when the value of the R-wave was 1 nT_{p-p}. However, we could not clearly observe the corresponding signal when the value of the R-wave was 100 pT_{p-p}. In order to suppress the noise component whose voltage was about 1 V_{p-p}, we decided to use an averaging technique. Fig. 25 shows examples of the waveform averaged 20 times. In this averaging, the applied current of MCG signal was used as a trigger signal. Even if the value of R-wave was 100 pT_{p-p}, we can find the corresponding signal of 1 V_{p-p}. From these results, we confirmed that the possibility to detect a MCG signal with this induction gradiometer.

6 MCG Measurement

It is a challenge to detect MCG signal without magnetically shielded environment. It is known that the typical value of magnetic field from human heart is a few hundred pT order. According to the electronics design, our developed induction gradiometer has sufficient sensitivity to detect the MCG signal. Although the measured signal was distorted, the output voltage was 1 V_{p-p} which corresponds to the value of the R-wave. The induction gradiometer allows us to detect an imbalance of magnetic flux in the pickup coil, and it has constant sensitivity when the frequency is larger than 18 Hz. However the corresponding magnetic noise of 60 Hz in our laboratory environment was about 0.68 nT_{p-p}. It was already confirmed that the digital filter is not enough to observe the MCG signal. In order to demonstrate real MCG measurement in our laboratory environment, we used averaging technique with ECG signal from a human heart as a trigger. We made instrumentation amplifiers for ECG measurement. The gain of the amplifiers was 100. For this measurement, a conventional bipolar lead (CM5) method with surface electrodes (Vitrode, Nihon koden) was used. The output signal was processed by digital filter after the voltage was recorded by LabVIEW. Digital filters are the same as those for the MCG measurement. Fig. 26 shows an example of the ECG measurement.

Fig. 27 shows a photograph of our experiment. A human subject lied on a wooden bed having a hole to hold the pickup coil of the induction gradiometer. The pickup coil was touched to the chest of the human subject. In order to suppress electrical interference to the pickup coil, the measurement was conducted inside the Faraday cage.

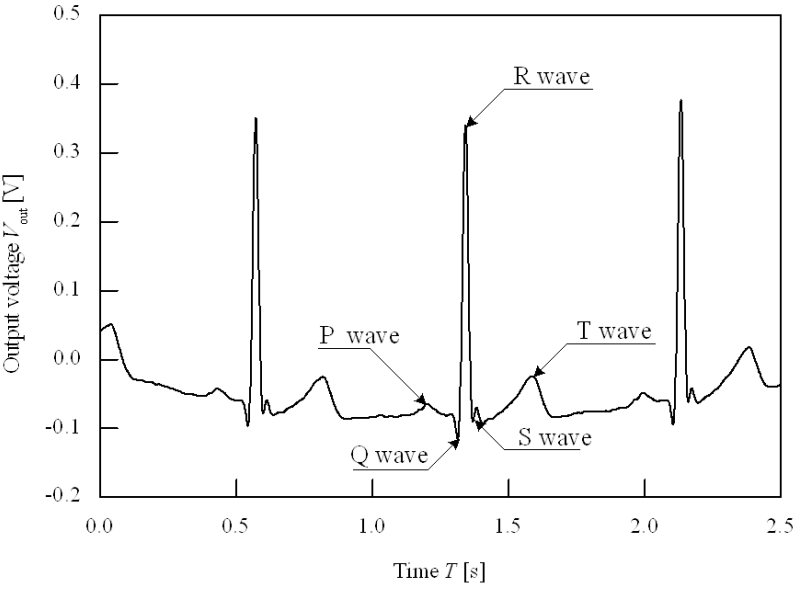

Fig. 26. An example of measured ECG signal from a human heart

Fig. 27. Experimental setup for ECG and MCG measurements from human heart

Fig. 28 shows an example of the measured waveforms of the MCG and ECG signals. As we expected, the noise component was about 1 $V_{p\text{-}p}$. In contrast, the red mark points were every time observed which corresponded to the ECG signal. Fig. 29 shows the waveforms averaged 100 times. We can find that the output voltage of 1.5 $V_{p\text{-}p}$ which corresponds to the ECG signal. According to the results with modelled MCG signal, it was an acceptable value because the corresponding R-wave peak was 150 $pT_{p\text{-}p}$.

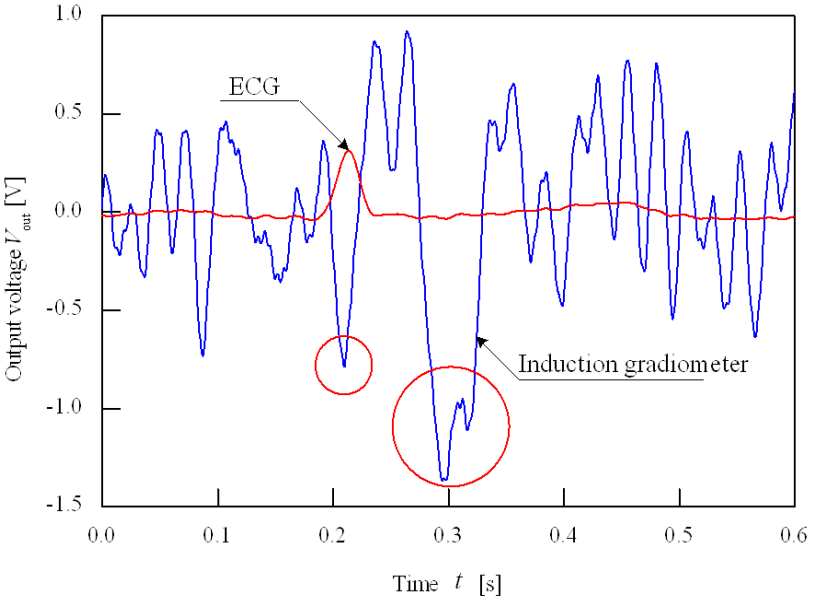

Fig. 28. An example of measured waveforms of MCG and ECG signal

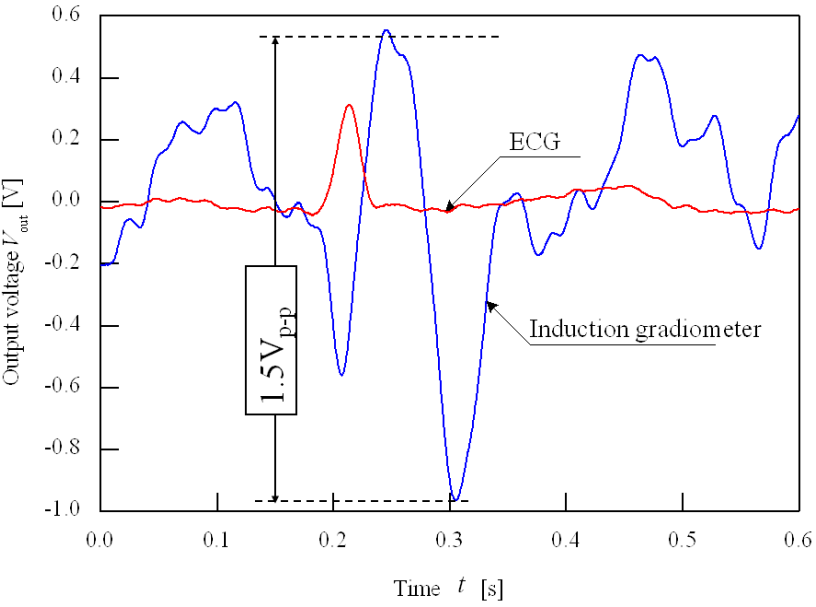

Fig. 29. An example of measured waveforms of MCG and ECG signal averaged 100 times

Fig. 30 shows an example of measured waveforms averaged 100 times without touching the pickup coil to the chest of the human subject. Because MCG signal can be observed near the surface of the human chest, it should not be observed a waveform which corresponds to ECG signal. At that time, the noise component in the output voltage was also about 1 $V_{p\text{-}p}$. It means that the noise environment was similar, and no electrical interference due to contact between human and pickup coil was found. In contrast, no typical profile was observed which corresponded to the ECG signal. From these results, we concluded that our developed induction gradiometer can detect magnetic fields from human heart.

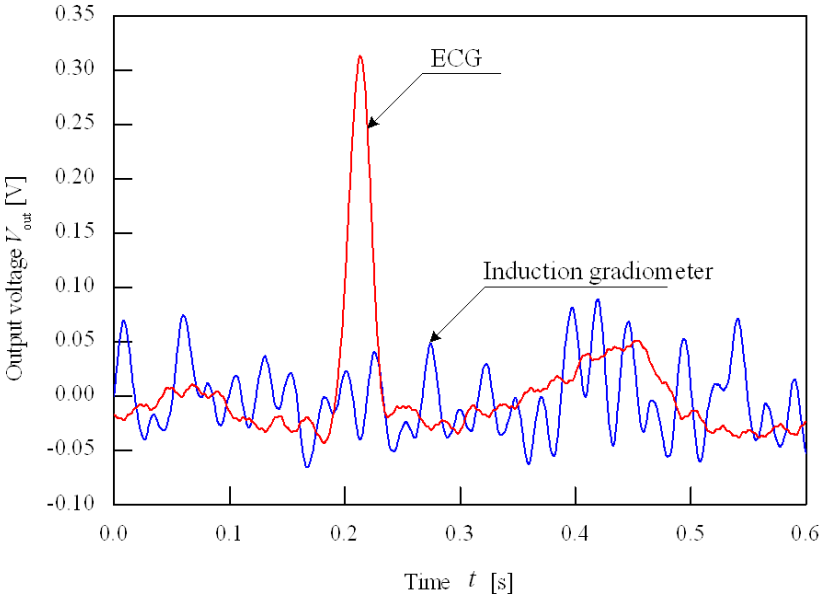

Fig. 30. An example of measured waveforms averaged 100 times. The chest of the human subject did not touch to the pickup coil of the induction gradiometer.

7 Conclusions

This paper has presented a design of an induction gradiometer for MCG measurement in a laboratory environment. It is a challenge to detect MCG signal with simple instrumentations. To detect MCG signal with an induction magnetometer in our laboratory environment, we have to reject both electrical interference and magnetic noise. Our proposed both current-to-voltage converter and grounding method effectively worked to suppress the electrical interference to the gradiometer. The differential structured pickup coil in the gradiometer allows us to suppress the magnetic noise component in the output voltage. It was less than 1 $nT_{p\text{-}p}$ in our laboratory environment. If we can use magnetically shielded

environment, the averaging technique is not required. It means that there is the possibility of simultaneous MCG measurement which is desired in clinical use. Although the detected signal was distorted by the phase profile in the electronics, an inverse filter could help to reconstruct the original MCG signal.

References

[1] Lenz, J., Edelstein, A.S.: Magnetic sensors and their applications. IEEE Sensors Journal 6, 631–649 (2006)

[2] Prance, R.J., Clark, T.D., Prance, H.: Compact broadband gradiometric induction magnetometer system. Sensors and Actuators a-Physical 76, 117–121 (1999)

[3] Tashiro, K.: Optimal design of an air-core induction magnetometer for detecting low-frequency fields of less than 1 pT. J. Magn. Soc. Jpn. 30, 439–442 (2006)

[4] Tashiro, K.: Broadband air-core Brooks-coil induction magnetometer. In: Proc. of SICE-ICASE International Joint Conference 2006, TA07-2 (2006)

[5] Tashiro, K.: Proposal of coil structure for air-core induction magnetometer. Proc. IEEE Sensor, 939–942 (2006)

[6] Tashiro, K., Wakiwaka, H., Kakiuchi, A., Matsuoka, A.: Comparative study of air-core coil design for induction magnetometer with current-to-voltage converter. In: Proc. of Second International Conference on Sensing Technology (ICST 2007), pp. 590–594 (2007)

[7] Tashiro, K., Inoue, S., Wakiwaka, H.: Sensitivity limits of a magnetometer with an air-core pickup coil. Sensors & Transducers Journal 9, 171–181 (2010)

[8] Inoue, S., Uchiyama, Y., Tashiro, K., Wakiwaka, H.: Observation of weak magnetic field in low-frequency range with portable induction magnetometer. Journal of the Japan Society of Applied Electromagnetics and Mechanics 19(supp.), 197–202 (2011)

[9] Grover, F.W.: Inductance Calculations. Dover Phoenix editions, pp. 94–113 (2004)

[10] Macintyre, S.A.: A portable low noise low frequency three-axis search coil magnetometer. IEEE Trans. Magn. 16, 761–763 (1980)

[11] Prance, R.J., Clark, T.D., Prance, H.: Compact room-temperature induction magnetometer with superconducting quantum interference device level field sensitivity. Rev. Sci. Instrum. 74, 3735–3739 (2003)

[12] Estola, K.P., Malmivuo, J.: Air-core induction-coil magnetometer design. J. Phys. E: Sci. Instrum. 15, 1110–1113 (1982)

[13] Korepanov, V., Berkman, R., Rakhlin, L., Klymovych, Y., Prystai, A., Marussenokov, A., Afanassenko, M.: Advanced field magnetometers comparative study. Measurement 29, 137–146 (2001)

[14] Sklyar, R.: Superconducting induction magnetometer. IEEE Sensors J. 6(2), 357–364 (2006)

[15] Tumanski, S.: Induction coil sensors - a review. Measurement Science & Technology 18, R31–R46 (2007)

[16] Tashiro, K., Kakiuchi, A., Moriizumi, K., Wakiwaka, H.: An Experimental Study of Stable Operating Conditions for a High-Sensitivity Induction Gradiometer. IEEE Trans. Magn. 45, 2784–2787 (2009)

[17] Baule, G., Mcfee, R.: Detection of Magnetic Field of Heart. American Heart Journal 66, 95–96 (1963)

[18] Cohen, D.: Magnetoencephalography: evidence of magnetic fields produced by alpha-rhythm currents. Science 161, 784–786 (1968)
[19] Sternickel, K., Braginski, A.I.: Biomagnetism using SQUIDs: status and perspectives. Superconductor Science & Technology 19, S160–S171 (2006)
[20] Koch, H.: SQUID Magnetocardiography: Status and Perspectives. IEEE Trans. Appl. Super. 11, 49–59 (2001)
[21] Tashiro, K., Wakiwaka, H., Inoue, S.: Electrical Interference with Pickup Coil in Induction Magnetometer. In: Proc. of the 2011 Fifth International Conference on Sensing Technology (ICST 2011), pp. 90–93 (2011)